ACES Asian Chemical Editorial Society

DOI: 10.1002/asia.201501366

CHEMISTRY AN ASIAN JOURNAL Full Paper

Electrochemistry

Pi-Extended Diindole-Fused Azapentacenone: Synthesis, Characterization, and Photophysical and Lithium-Storage Properties

Jianfeng Zhao,[a, b] Renping Li,[a] Wei Ai,[c] Dai Dong,[a] Jiewei Li,[a] Lin Chen,[d] Linghai Xie,*[b] Ting Yu,*[c] and Wei Huang*[a, b]

Abstract: **Pi**-extended polyaromatics tend to exhibit improved electronic properties with respect to the intrinsic structures. Herein, the rational design of a π-extended diindole-fused diazapentacenone (**IP**), with a nine-ring-fused core, obtained by applying an intramolecular Friedel–Crafts diacylation synthetic routine, is reported. The chemical structure, physical properties, and morphology of **IP** were fully characterized. Serving as an organic cathode material for a lithium-ion battery, the as-prepared nanorods of π-extended **IP** display higher conductivity and superior electrochemical performance than those of the naked diazapentacenone without diindole fusion.

Introduction

Pi-extended polyaromatics have attracted increasing attention in recent decades owing to their potential applications in organic electronics[1] and energy-storage devices.[2] The planarity and rigidity of multiring-fusion of the π-conjugated backbones of these π-extended aromatic molecules may enhance or enrich their abundant optophysical properties, including absorbance, quantum efficiency, charge mobility, environmental stability, and crystallinity.[3] Therefore, the development of a facile and effective strategy for fabricating novel π-extended polyaromatic derivatives is highly desirable, but remains a challenge. To this end, various one-step fusion synthetic approaches have been developed to achieve large π-extended polyaromatics as electron-rich[4] or -deficient organic semiconductors.[5] In particular, large π-extended diazapentacenone derivatives have been widely explored as highly efficient dopants, green-light emitters,[6] and effective charge carriers.[7] However, the lithium-ion storage properties of π-extended azapentacenone derivatives with versatile carbonyl groups have rarely been reported.[8] It is believed that stronger intermolecular interactions among large molecular π surfaces, in synergy with electron-donatable sp^3-N, could induce the effective self-assembly of **IP** molecules; hence, facilitating intermolecular charge injection and transportation, and consequently, overcoming intrinsic electron insulation.[9] In addition, the embedding of carbonyl groups into the large conjugated framework results in the formation of a stable structure that can potentially promote the Li^+ insertion/deinsertion reaction through the known enolization process.[2a, 10]

Herein, a novel π-extended diindole-fused diazapentacenone, indolo[1,2,3-*fg*]indolo[3′,2′,1′:8,1]quinolino[2,3-*b*]acridine-8,18-dione (**IP**; Scheme 1a), has been designed and synthesized through intramolecular Friedel–Crafts diacylation. The nine-ring-fused **IP** core with two end-fused indoles is electrochemically active and is able to capture lithium through a chemical reaction between Li^+ and the carbonyl groups. The structural and physical properties of **IP** were systematically characterized by ^{1}H NMR spectroscopy, high-resolution mass spectrometry, UV/Vis spectroscopy, fluorescence spectroscopy, transient fluorescence spectroscopy, elemental analysis, and theoretical calculations. ^{13}C NMR spectroscopy is not available owing to low solubility in $CDCl_3$/CF_3COOD and other common organic solvents. Moreover, a recrystallization technique was further applied to convert the as-prepared **IP** into a nanorod structure, as confirmed by XRD, field-emission (FE) SEM, and

[a] *Prof. J. Zhao, R. Li, D. Dong, J. Li, Prof. W. Huang*
Key Laboratory of Flexible Electronics (KLOFE) and
Institute of Advanced Materials (IAM)
Jiangsu National Synergetic Innovation Center
for Advanced Materials (SICAM)
Nanjing Tech University (NanjingTech)
30 South Puzhu Road, Nanjing 211816 (P.R. China)
E-mail: iamwhuang@njtech.edu.cn

[b] *Prof. J. Zhao, Prof. L. Xie, Prof. W. Huang*
Key Laboratory for Organic Electronics and
Information Displays (KLOEID) and Institute of Advanced Materials
Nanjing University of Posts & Telecommunications
Nanjing 210023 (P.R. China)
E-mail: iamlhxie@njupt.edu.cn

[c] *W. Ai, Prof. T. Yu*
Division of Physics and Applied Physics
School of Physical and Mathematical Sciences
Nanyang Technological University
637371 (Singapore)
E-mail: yuting@ntu.edu.sg

[d] *L. Chen*
Nanjing Polytechnic Institute
Nanjing 210048 (P.R. China)

Supporting information for this article is available on the WWW under http://dx.doi.org/10.1002/asia.201501366.

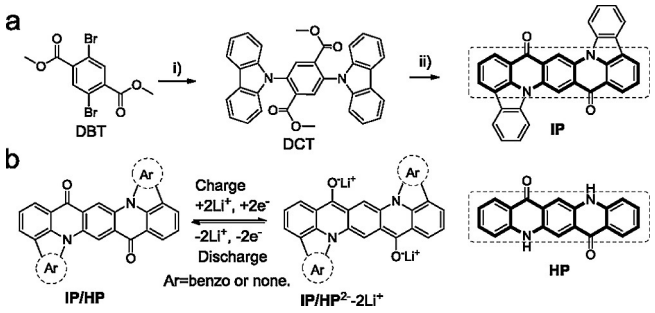

Scheme 1. The synthetic routine to **IP** and molecular structure of quinolino[2,3-*b*]acridine-7,14(5*H*,12*H*)-dione (**HP**). a) i) CuI, K_2CO_3, [18]crown-6, carbazole, *o*-dichlorobenzene (*o*-DCB), 180 °C, N_2, 24 h; ii) 1) NaOH/MeOH, reflux, 10 h; $HCl_{(aq)}$, $SOCl_2$/DMF (cat.), reflux, 12 h; 2) $AlCl_3/CH_2Cl_2$, RT, 12 h. Dashed squares indicate the azapentacene backbone. b. Scheme of the proposed mechanism for Li^+ insertion/deinsertion in **IP/HP**.

TEM. Notably, the **IP** nanorods illustrate different lithium storage performance compared with that of commercially available **HP** (Scheme 1 b). The embedded carbonyl groups on the **IP** ring could promote the redox enolation reaction; thus playing an important role in reversible Li^+ insertion/deinsertion.

Results and Discussion

Synthesis

The traditional synthetic routine to a soluble diazapentacenone analogue is a four-step procedure,[6f,11,12] which involves high-temperature (260 °C)/nitrobenzene conditions and strong base treatment to dehydrolyze precursors to give the final product. Herein, we designed a synthetic route starting from commercially available DBT (Scheme 1) and carbazole to achieve the novel **IP** through a typical copper(I)-catalyzed Ullmann reaction. Then, high-yielding demethylation, chlorination, and a key intramolecular Friedel–Crafts diacylation step were applied sequentially. The obtained **IP** powder was further washed, under sonication, with various solvents, including acetone, methanol, *N*,*N*-dimethylformamide (DMF), and Soxhlet extraction in CH_2Cl_2, in turn, and finally treated with a recrystallization step from *o*-DCB.

Photophysical Properties

The UV/Vis absorption and fluorescence spectra and emission decay curve of **IP** are presented in Figure 1. The UV/Vis absorption spectrum (Figure 1 a, excited at $\lambda = 365$ nm) of **IP** in *o*-DCB (1.0×10^{-5} mol L^{-1}) exhibits an absorption maximum (λ_{max}) at $\lambda = 498$ nm, which can be assigned to an electronic π–π^* transition of the planar conjugated backbone, resulting in a calculated optical band gap of 2.49 eV. A strong emission at $\lambda =$ 510 nm and a shoulder at $\lambda = 543$ nm were observed, which presented pure green fluorescence. Compared with the emission maximum at $\lambda = 510$ nm, the Stokes shift was calculated to be as small as 12 nm owing to the strong rigid conjugated backbone.[11] The normalized emission decay curve for **IP** in *o*-DCB (1.0×10^{-5} mol L^{-1}) and corresponding decay fitting are

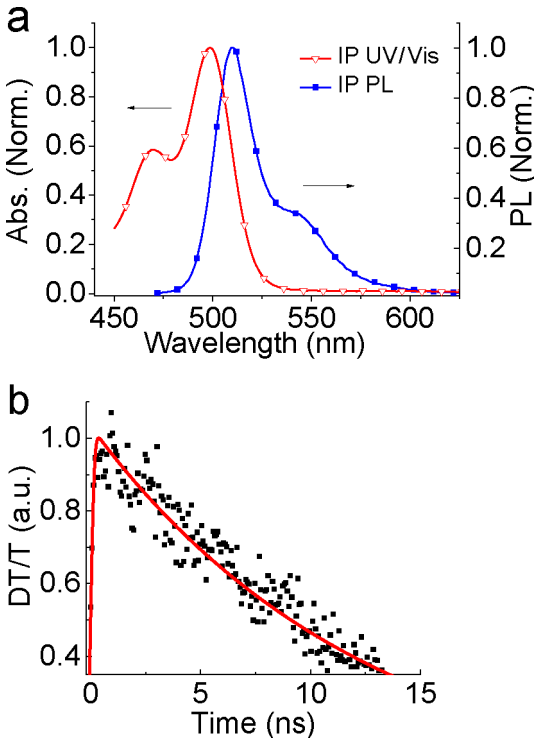

Figure 1. a) UV/Vis absorption and photoluminescence (PL) spectra of **IP** in *o*-DCB (10^{-5} mol L^{-1}). b) Normalized emission decay curve for **IP** in *o*-DCB (10^{-5} mol L^{-1}).

shown in Figure 1 b. The intensity decays with time through a single-exponential function, with a well-defined value of χ^2 (0.97064) and fitted decay lifetimes as long as 12.56 ns. Therefore, the **IP** molecule possesses as long a photoluminescent lifetime as other azapentacenones.[6g] The rigid backbone was also confirmed by the long fitted decay lifetimes and narrow UV/Vis absorbance and PL bands. Therefore, the insolubility of **IP** molecules in the organic electrolyte is enhanced by strong intermolecular π–π stacking, which leads to improved intermolecular charge-transfer abilities.

Theoretically, the planar conjugated structure of **IP** was a local minimum because there were no imaginary frequencies in the harmonic vibrational analysis with the 6-31G(d) basis set. The theoretical value of the HOMO/LUMO (−5.56/−2.43 eV) band gap was 3.13 eV (Figure 2). Because of the two fused indoles and two central carbonyl groups, the large hole and electron affinities of ambipolar **IP** molecule are favorable for both hole and electron injection in ambient, stable devices.[5e,13,14]

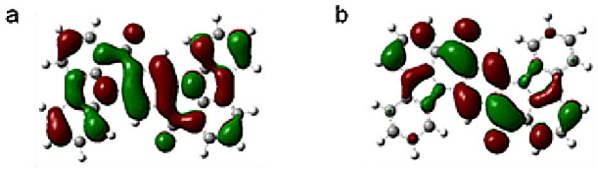

Figure 2. Wave functions for the a) HOMO (−5.56 eV) and b) LUMO (−2.43 eV) of the **IP** molecule.

Morphology

Large π-extended **IP** molecules have a strong tendency to form self-assembled nanostructures with good crystalline properties to facilitate charge transfer in the aggregates, as driven by intermolecular π–π stacking and van der Waals forces. Therefore, the **IP** molecules directly precipitated in the form of self-assembled nanorods during recrystallization. The obtained nanorods were observed through FE-SEM and TEM (Figure 3). Figure 3a and c presents typical FE-SEM and TEM morphologies of **IP** nanorods; the diameters of which cover the range of about 50–500 nm and lengths range from about 500 nm to 5 μm, owing to the rapid evaporation of *o*-DCB. Figure 3b and d presents typical FE-SEM and TEM morphologies of commercially available **HP** nanorods, which have uniform diameters in the range of about 50–100 nm and lengths ranging from about 100 to 200 nm. Nanorods of **IP** and **HP** both exhibit smooth, clean surfaces and crystalline forms. The **IP** and **HP** nanorods were also characterized by powder XRD. As shown in inset in Figure 3a, the main peaks at $2\theta = 7.6$, 11.58, 12.52, 25.26, and 26.77° give crystalline interplane distances of 1.162, 0.764, 0.706, 0.352, and 0.333 nm, respectively, according to Bragg's law: $2d\sin\theta = n\lambda$ ($\lambda = 1.540562$ Å). These distances result from the ordered packing of **IP** molecules; thus indicating the high crystallinity of **IP** aggregates. The polarized optical microscopy image of **IP** nanorods indicates that **IP** molecules stack anisotropically in the crystals (Figure S4, right, in the Supporting Information).[12] The successful preparation of **IP** nanorods would potentially enhance the performance of the electrode as a cathode material for lithium-ion batteries.

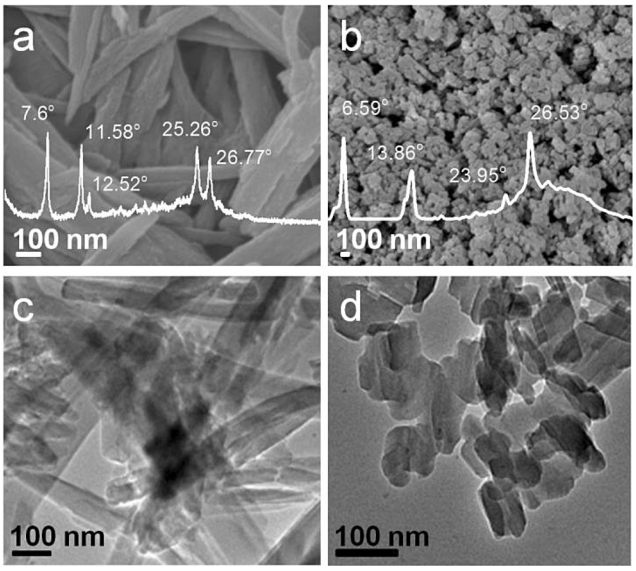

Figure 3. FE-SEM (a, b) and TEM (c, d) images of self-assembled **IP** (a, c) **HP** (b, d) nanorods. Insets: XRD patterns of the **IP** and **HP** nanorods.

Electrochemical Performance

Figure 4 shows the electrochemical lithium storage performance of **IP**/**HP** by using the standard half-cell configuration.[9b,15] As shown in Figure 4a, the cells were first discharged (Li^+ inserted) to 1.5 V and then charged (Li^+ released) to 4.5 V at a constant current of 50 mA g^{-1}. During discharging, each carbonyl group of the reduced **IP** molecule can accept one electron and combine with one Li^+ to form a lithium-enolated cyclohexa-1,4-diene structure (**IP**/**HP**$^{2-}$–2Li^+; Li^+ insertion), whereas the charging process proceeds with a Li^+ deinsertion step to give a reconstituted diketone structure (Scheme 1b). Although the large initial irreversible specific charge capacity of 444 mA h g^{-1} of the **IP** electrode is similar to that of the **HP** electrode (460 mA g^{-1}; Figure S9 in the Supporting Information), its initial irreversible specific discharge capacity still reaches a value that is 175 mA h g^{-1} higher than that of the **HP** electrode (135 mA h g^{-1}). Their irreversibility can most likely be ascribed to the strong trend of less-lithiated, amorphous **IP** and **HP** molecules on the surface of the nanorods dissolving in the electrolyte.[9b,16,17] However, the decreased capacities exhibit as-predicted stability and reversibility after the first few cycles. The initial reversible charge/discharge specific capacities of the **IP** electrode retain 266 and 147 mA h g^{-1}, which are 1.5/1.2 times that of 170 and 116 mA h g^{-1} for the **HP** electrode. After 150 cycles, the reversible specific charge/discharge capacity retentions of the **IP** electrode show values of 103 and 100 mAh g^{-1}, which are both 1.2 times higher than the values of 82 and 81 mAh g^{-1} for the **HP** electrode, respectively. The **IP** electrode appears to exhibit a strong competitive advantage over the **HP** electrode. Meanwhile, the coulombic efficiencies (Figure S9 in the Supporting Information) in the 150th cycle tend to be very close (95.41 and 99.28%).

In Figure 4b, the line composed of squares shows the discharge rate performance of the **IP** electrode. The corresponding rate capacities with cycle numbers are 148.6/6th, 110.2/12th, 84.7/18th, 64.3/24th, 102.4/30th, and 127.8/36th mA h g^{-1} at specific current densities of 50, 100, 200, 400, 100, and 50 mA g^{-1}, respectively. Interestingly, even at the highest current density of 400 mA g^{-1}, the **IP** electrode can still deliver 64.3 mAh g^{-1}. Most importantly, when the current density is adjusted to be 50 mA g^{-1} at the 36th cycle, the measured discharge capacity was 127.8 mA h g^{-1}, which recovered to almost the same value as that of the initial capacity in the first cycle. A set of lower capacities are compatible with the **IP** electrode and demonstrate the better rate performance of the **IP** electrode. The corresponding voltage profiles (Figure 4c and Figure S10 in the Supporting Information) exhibit similar electrochemical properties with similar charge/discharge voltage–capacity curves at the four different current densities. Meanwhile, the dashed lines in Figure 4c and Figure S10 in the Supporting Information indicate the two slopes without clear plateaus in the discharge process for the **IP** electrode, which imply a reversible mechanism for the 2Li^+ insertion/deinsertion process. A similar two-slope curve of the **HP** electrode further confirms the mechanism.

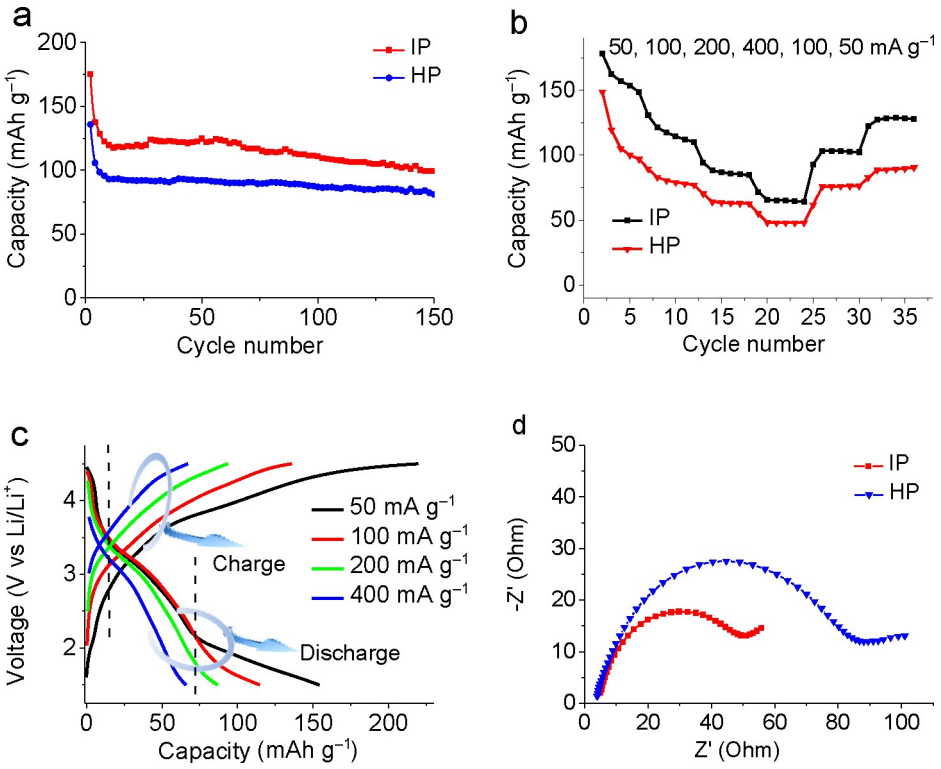

Figure 4. a) Discharging curves of the **IP/HP** nanorod electrodes tested at a current density of 50 mA g^{-1}. b) Discharge rate performance of the **IP/HP** electrodes at various current densities and cycles. c) Discharge–charge curves of **IP** electrodes at various current densities. Dashed lines indicate the turning point of different slopes in the discharging process. d) Electrochemical impedance spectroscopy (EIS) results for the **IP/HP** electrodes.

To further confirm the stronger charge-transfer ability and to determine the most rational reason for the better performance of the **IP** electrode than that of the **HP** electrode, we carried out an EIS test on the **IP** and **HP** electrodes under the same EIS testing conditions, including carbon black ratio, additive, dispersion solvent, and drying time in the oven. The charge-transfer resistance result is depicted in Figure 4d. It can be seen that both **IP** and **HP** electrodes exhibit a small semicircle in the high-frequency region, which corresponds to the charge-transfer process. The low-frequency region of the EIS plots suggests that the **IP** electrode exhibits a much lower Li^+ diffusion resistance than that of the **HP** electrode. Notably, the charge-transfer resistance of the **IP** electrode is about 46.4 Ω, which is much smaller than the value of about 84.1 Ω for the **HP** electrode; this indicates better conductivity of the **IP** electrode under the same EIS testing conditions. Furthermore, the reasons for better conductivity with a lower charge-transfer resistance for the **IP** electrode, compared with that of **HP**, are most likely 1) the structurally larger π-conjugated surface, and 2) the naked backbone of **IP** molecule without steric hindrance from substituents, leading to well-crystallized intermolecular π–π stacking to facilitate charge transfer. Therefore, the better lithium storage properties of the **IP** electrode can be attributed to the molecular π-extended skeleton, which can ensure good electron and Li^+ transportation in the nanostructures. The diindole-fused π-extended microstructure exerts an effective influence on the macroproperties. The experimental results demonstrate that π-extended azapentacenone derivative **IP** is more useful than **HP** as a high-performance lithium storage cathode material.

Conclusion

A well-designed, larger, π-extended diazapentacenone derivative **IP** and its self-assembled nanorods have been successfully obtained and explored as a cathode for a lithium storage material. The nine-ring-fused framework of symmetrical **IP** possesses three pre-embedded elements, including π extension, two carbonyl groups, and sp^3-N, obtained through a key intramolecular Friedel–Crafts diacylation reaction. From the presented data and analysis, including better specific capacities, rate capabilities, and cyclabilities, the nanostructured **IP** electrode is a better π-extended carbonyl electrode than that of **HP**. The advantages of a large, π-extended diazapentacenone as a novel organic energy-storage system for lithium storage has been demonstrated. Further work is in progress is to develop much larger π-extended derivatives with better performance for high-capacity, high-power lithium-ion batteries.

Experimental Section

Materials

Dimethyl 2,5-dibromoterephthalate and carbazole were purchased from Beijing dtftchem Technology Co., Ltd. The **HP** (98%) compound was purchased from Nanjing DeBioChem Co., Ltd. Other re-

agents and solvents were purchased from Sigma–Aldrich. All solvents were used without further purification.

Synthesis of DCT

A mixture of dimethyl 2,5-dibromoterephthalate (3.49 g, 0.01 mol), carbazole (3.5 g, 0.021 mol), *o*-DCB (15 mL), K_2CO_3 (2.9 g, 0.02 mol), [18]crown-6 (530 mg, 2 mmol), and CuI (390 mg, 2 mmol) were added to a flask (50 mL) under a nitrogen atmosphere and heated at reflux for 24 h. The mixture was cooled to room temperature and washed with CH_2Cl_2. The solvent was removed in vacuum. Hexane (100 mL) was added and the solution was allowed to stand for several hours. The precipitated crude product was filtered and purified by column chromatography with petroleum ester/ethyl acetate (PE/EA) as the eluent (6:1). DCT was recrystallized from PE/EA as yellow–green crystals (3.98 g, 7.4 mmol, 76%). M.p. 239 °C; ^{1}H NMR (400 MHz, $CDCl_3$): $\delta = 8.34$ (s, 2H), 8.17 (d, $J = 7.716$ Hz, 4H), 7.46 (m, 4H), 7.34 (t, $J = 7.329$ Hz, 4H), 7.31 (d, $J = 8.073$ Hz, 4H), 3.28 ppm (s, 6H); ^{13}C NMR (100 MHz, $CDCl_3$): $\delta = 164.9$, 141.3, 136.5, 134.3, 133.5, 126.3, 123.7, 120.6, 120.5, 109.2, 52.7 ppm; GC-MS (EI): *m/z*: 524.1 $[M]^+$; elemental analysis calcd (%) for $C_{34}H_{24}N_2O_4$: C 77.85, H 4.61, N 5.34; found: C 77.92, H 4.78, N 5.43.

CCDC 921472 contains the supplementary crystallographic data for this paper. These data can be obtained free of charge from The Cambridge Crystallographic Data Centre.

Synthesis of IP

DCT (2.62 g, 5 mmol), NaOH (0.44 g, 0.011 mol), and methanol (20 mL) were heated at reflux for 10 h. After cooling to room temperature, water was added and the mixture was acidified to pH 1–2. A yellow powder was collected by filtration and dried in a vacuum oven. Then the yellow powder was heated at reflux in $SOCl_2$ (1 drop of DMF) for another 10 h. Following the distillation of $SOCl_2$ under reduced pressure, $AlCl_3$ (1.45 g, 0.011 mol) and dry CH_2Cl_2 (15 mL) were added to the flask with agitation for 12 h under ambient conditions. Moisture was prevented from entering the flask through the addition of a dry tube filled with anhydrous $CaCl_2$. Water was added to the mixture portionwise and the product was collected by vacuum filtration. The filtrate cake was dried and ground for 20 min to give a powder that was washed sequentially by HCl (1 M), water, MeOH, acetone, and $CHCl_3$ under ultrasonication, followed by Soxhlet extraction with CH_2Cl_2 for a week. The obtained **IP** product was finally collected as a reddish orange powder (1.7 g, 3.7 mmol, 72%). M.p. >300 °C; ^{1}H NMR (400 MHz, $CDCl_3/CF_3COOD$): $\delta = 9.56$ (s, 2H), 8.44–8.47 (m, 6H), 8.13 (d, $J = 7.453$ Hz, 2H), 7.72–7.76 (t, $J = 7.744/7.760$ Hz, 4H), 7.53 ppm (t, $J = 7.349/7.390$ Hz, 2H); MALDI-TOF MS: *m/z*: 460.21 $[M^+]$; HRMS: *m/z* calcd for $C_{32}H_{17}N_2O_2$ $[M+H]^+$: 460.1212; found: 461.1184; elemental analysis calcd (%) for $C_{32}H_{16}N_2O_2$: C 83.47, H 3.50, N 6.08; found: C 83.59, H 3.64, N 6.21.

Methods

Solution ^{1}H NMR spectra were measured on a Bruker ARX 400 spectrometer. The UV/Vis absorption and fluorescence spectra were recorded on Shimadzu UV-2501 and RF-5301 spectrophotometers, respectively. MS were collected on a MALDI TOF2 AXIMA mass spectrometer. High-resolution MALDI TOF mass spectra were recorded on a Waters Q-Tof premier TM mass spectrometer. Elemental analyses were performed on an elementar Analysensysteme GmbH-vario EL III element analyzer. DFT at the B3LYP/6-31G(d)[18] level was applied to optimize the geometry of the rigid **IP** molecular structure. Gaussian 09[19] code was used to relax the structure fully.[20] The as-prepared nanorods were coated with platinum in an ion coater for 60 s before FE-SEM imaging. The sizes and shapes of the nanorods were observed on a JSM-6700F field-emission scanning electron microscope (JEOL) at an accelerating voltage of 5 kV. Fluorescence decay lifetimes were measured by exciting the sample with a laser flash-photolysis spectrometer (LKS.60, Applied Photophysics), equipped with a Q-switched Nd:YAG laser (Brilliant B, Quantel), a 150 W pulsed Xe lamp, and an R928 photomultiplier, which was used to record nanosecond-difference absorption spectra. Samples were excited at $\lambda = 400$ nm, and each time-resolved trace was acquired by averaging 10 laser shots at a repetition rate of 1 Hz. The room-temperature fluorescence decay was measured by exciting the samples in *o*-DCB (1.0×10^{-5} mol L^{-1}) with $\lambda =$ 400 nm, 150 fs, laser pulses. These laser pulses were generated from a Coherent TOPAS-C optical parametric amplifier that was pumped by using a 1 kHz Coherent Legend regenerative amplifier, which was seeded by an 80 MHz Coherent Vitesse oscillator. The laser pulses were focused by a lens ($f = 25$ cm) on the solution in a 2 mm thick quartz cell. The emission from the samples was collected at a backscattering angle of 150° by means of a pair of lenses and directed into an Optronis Optoscope streak camera system, which had an ultimate temporal resolution of 10 ps.

Electrochemical Tests

Conductive carbon was added to improve utilization of the carbonyl groups. The cathodes were fabricated by blending the as-obtained samples of **IP/HP** nanorods, carbon black, and polyvinylidene fluoride (PVDF) in *N*-methyl-2-pyrrolidone, with a weight ratio of 60:30:10. The obtained slurry was pasted onto an aluminum foil and dried at 100 °C for 12 h in a vacuum oven. Lithium metal was simultaneously used as the counter anode and reference electrode. The electrolyte was 1.0 M $LiPF_6$ in a solution of ethylene carbonate and dimethyl carbonate. The cathode and anode were assembled into coin cells in an argon-filled glove box with both moisture and oxygen contents below 0.1 ppm. The galvanostatic charge/discharge tests of the assembled cells were performed by using a NEWARE battery-testing system between 1.5 and 4.5 V at different rates. The capacity values were calculated based on the weight of nanorod materials loaded on the aluminum foil. The alternating current (AC) impedance measurements were carried out at room temperature on a CHI 760D electrochemical workstation (CH Instruments, Inc.). EIS was performed with an AC voltage of 5 mV amplitude in the frequency range from 100 kHz to 10 mHz.

Acknowledgements

We thank the 973 program (2015CB932200), the National Natural Science Foundation of China (NSFC, 21502091 and 61274065, 21003706, 21274064, 21144004, 60876010, 61177029, 20774043, 20704023, and 20974046), and the Natural Science Foundation of Jiangsu Province (BK20130912 and 14KJB430017) for financial support.

Keywords: charge transfer · conjugation · electrochemistry · lithium · polyaromatics

[1] a) U. H. F. Bunz, *Acc. Chem. Res.* **2015**, *48*, 1676–1686; b) J. Li, Q. Zhang, *ACS Appl. Mater. Interfaces* **2015**, *7*, 28049–28062; c) D. Larcher, J. M. Tarascon, *Nat. Chem.* **2015**, *7*, 19–29; d) Q. Miao, *Adv. Mater.* **2014**, *26*, 5541–5549; e) U. H. Bunz, J. U. Engelhart, B. D. Lindner, M. Schaffroth,

Angew. Chem. Int. Ed. **2013**, *52*, 3810 – 3821; *Angew. Chem.* **2013**, *125*, 3898 – 3910; f) K. Cai, J. Xie, D. Zhao, *J. Am. Chem. Soc.* **2014**, *136*, 28 – 31.

[2] a) M. Park, D. S. Shin, J. Ryu, M. Choi, N. Park, S. Y. Hong, J. Cho, *Adv. Mater.* **2015**, *27*, 5141 – 5146; b) J. Wu, X. Rui, C. Wang, W. B. Pei, R. Lau, Q. Yan, Q. Zhang, *Adv. Energy Mater.* **2015**, DOI: 10.1002/aenm.201402189; c) Y. Liang, Z. Chen, Y. Jing, Y. Rong, A. Facchetti, Y. Yao, *J. Am. Chem. Soc.* **2015**, *137*, 4956 – 4959; d) S. Yuan, Y.-B. Liu, D. Xu, D.-L. Ma, S. Wang, X.-H. Yang, Z.-Y. Cao, X.-B. Zhang, *Adv. Sci.* **2015**, *2*, DOI: 10.1002/advs.201400018; e) C. Luo, R. Huang, R. Kevorkyants, M. Pavanello, H. He, C. Wang, *Nano Lett.* **2014**, *14*, 1596 – 1602; f) S. Yuan, X.-l. Huang, D.-l. Ma, H.-G. Wang, F.-Z. Meng, X.-B. Zhang, *Adv. Mater.* **2014**, *26*, 2273 – 2279; g) Y. Liang, P. Zhang, S. Yang, Z. Tao, J. Chen, *Adv. Energy Mater.* **2013**, *3*, 600 – 605; h) X. Han, F. Yi, T. Sun, J. Sun, *Electrochem. Commun.* **2012**, *25*, 136 – 139; i) Z. Hong, M. Wei, T. Lan, L. Jiang, G. Cao, *Energy Environ. Sci.* **2012**, *5*, 5408 – 5413.

[3] a) C. Wang, J. Zhang, G. Long, N. Aratani, H. Yamada, Y. Zhao, Q. Zhang, *Angew. Chem. Int. Ed.* **2015**, *54*, 6292 – 6296; *Angew. Chem.* **2015**, *127*, 6390 – 6394; b) H.-G. Wang, S. Yuan, Z. Si, X.-B. Zhang, *Energy Environ. Sci.* **2015**, *8*, 3160 – 3165; c) K. Liu, C.-L. Song, Y.-C. Zhou, X.-Y. Zhou, X.-J. Pan, L.-Y. Cao, C. Zhang, Y. Liu, X. Gong, H.-L. Zhang, *J. Mater. Chem. C* **2015**, *3*, 4188 – 4196; d) S. More, S. Choudhary, A. Higelin, I. Krossing, M. Melle-Franco, A. Mateo-Alonso, *Chem. Commun.* **2014**, *50*, 1976 – 1979; e) J. U. Engelhart, O. Tverskoy, U. H. F. Bunz, *J. Am. Chem. Soc.* **2014**, *136*, 15166 – 15169; f) Y.-Y. Liu, C.-L. Song, W.-J. Zeng, K.-G. Zhou, Z.-F. Shi, C.-B. Ma, F. Yang, H.-L. Zhang, X. Gong, *J. Am. Chem. Soc.* **2010**, *132*, 16349 – 16351.

[4] a) Y. Yuan, G. Giri, A. L. Ayzner, A. P. Zoombelt, S. C. B. Mannsfeld, J. Chen, D. Nordlund, M. F. Toney, J. Huang, Z. Bao, *Nat. Commun.* **2014**, *5*, 3005; b) K. S. Park, S. M. Salunkhe, I. Lim, C. G. Cho, S. H. Han, M. M. Sung, *Adv. Mater.* **2013**, *25*, 3351 – 3356; c) J. Xiao, H. M. Duong, Y. Liu, W. Shi, L. Ji, G. Li, S. Li, X.-W. Liu, J. Ma, F. Wudl, Q. Zhang, *Angew. Chem.* **2012**, *124*, 6198 – 6202; d) T. V. Pho, J. D. Yuen, J. A. Kurzman, B. G. Smith, M. S. Miao, W. T. Walker, R. Seshadri, F. Wudl, *J. Am. Chem. Soc.* **2012**, *134*, 18185 – 18188; e) R. R. Parkhurst, T. M. Swager, *J. Am. Chem. Soc.* **2012**, *134*, 15351 – 15356; f) W.-Y. Lai, R. Xia, Q.-Y. He, P. A. Levermore, W. Huang, D. D. C. Bradley, *Adv. Mater.* **2009**, *21*, 355 – 360; g) J. E. Anthony, *Angew. Chem. Int. Ed.* **2008**, *47*, 452 – 483; *Angew. Chem.* **2008**, *120*, 460 – 492.

[5] a) T. He, M. Stolte, C. Burschka, N. H. Hansen, T. Musiol, D. Kälblein, J. Pflaum, X. Tao, J. Brill, F. Würthner, *Nat. Commun.* **2015**, *6*, 5954; b) J. Zhao, J. I. Wong, J. Gao, G. Li, G. Xing, H. Zhang, T. C. Sum, H. Y. Yang, Y. Zhao, S. L. A. Kjelleberg, *RSC Adv.* **2014**, *4*, 17822 – 17831; c) Y. Zhang, D. Hanifi, E. Lim, S. Chourou, S. Alvarez, A. Pun, A. Hexemer, B. Ma, Y. Liu, *Adv. Mater.* **2014**, *26*, 1223 – 1228; d) Z. Sun, Q. Ye, C. Chi, J. Wu, *Chem. Soc. Rev.* **2012**, *41*, 7857 – 7889; e) A. Lv, S. R. Puniredd, J. Zhang, Z. Li, H. Zhu, W. Jiang, H. Dong, Y. He, L. Jiang, Y. Li, W. Pisula, Q. Meng, W. Hu, Z. Wang, *Adv. Mater.* **2012**, *24*, 2626 – 2630; f) G. Li, Y. C. Wu, J. K. Gao, C. Y. Wang, J. B. Li, H. C. Zhang, Y. Zhao, Y. L. Zhao, Q. C. Zhang, *J. Am. Chem. Soc.* **2012**, *134*, 20298 – 20301; g) K. Cai, Q. Yan, D. Zhao, *Chem. Sci.* **2012**, *3*, 3175 – 3182; h) Y. Zhang, D. Hanifi, S. Alvarez, F. Antonio, A. Pun, L. M. Klivansky, A. Hexemer, B. W. Ma, Y. Liu, *Org. Lett.* **2011**, *13*, 6528 – 6531; i) D. Hanifi, D. Cao, L. M. Klivansky, Y. Liu, *Chem. Commun.* **2011**, *47*, 3454 – 3456; j) J. E. Anthony, A. Facchetti, M. Heeney, S. R. Marder, X. Zhan, *Adv. Mater.* **2010**, *22*, 3876 – 3892; k) E. Ahmed, T. Earmme, G. Q. Ren, S. A. Jenekhe, *Chem. Mater.* **2010**, *22*, 5786 – 5796.

[6] a) C. Wang, K. Wang, Q. Fu, J. Zhang, D. Ma, Y. Wang, *J. Mater. Chem. C* **2013**, *1*, 410 – 413; b) C. G. Wang, S. Y. Chen, K. Wang, S. S. Zhao, J. Y. Zhang, Y. Wang, *J. Phys. Chem. C* **2012**, *116*, 17796 – 17806; c) H. Bi, K. Ye, Y. Zhao, Y. Yang, Y. Liu, Y. Wang, *Org. Electron.* **2010**, *11*, 1180 – 1184; d) E. B. Faulkner, R. J. Schwartz, *High Performance Pigments*, Wiley-VCH, Weinheim, **2009**; e) J. Wang, Y. F. Zhao, C. D. Dou, H. Sun, P. Xu, K. Q. Ye, J. Y. Zhang, S. M. Jiang, F. Li, Y. Wang, *J. Phys. Chem. B* **2007**, *111*, 5082 – 5089; f) K. Q. Ye, J. Wang, H. Sun, Y. Liu, Z. C. Mu, F. Li, S. M. Jiang, J. Y. Zhang, H. X. Zhang, Y. Wang, C. M. Che, *J. Phys. Chem. B* **2005**, *109*, 8008 – 8016; g) J. A. Smith, R. M. West, M. Allen, *J. Fluoresc.* **2004**, *14*, 151 – 171.

[7] a) H.-J. Song, D.-H. Kim, E.-J. Lee, D.-K. Moon, *J. Mater. Chem. A* **2013**, *1*, 6010 – 6020; b) H. Li, C. Gu, L. Jiang, L. Wei, W. Hu, H. Fu, *J. Mater. Chem. C* **2013**, *1*, 2021 – 2027; c) E. D. Głowacki, M. Irimia-Vladu, M. Kaltenbrunner, J. Gsiorowski, M. S. White, U. Monkowius, G. Romanazzi, G. P. Suranna, P. Mastrorilli, T. Sekitani, S. Bauer, T. Someya, L. Torsi, N. S. Sariciftci, *Adv. Mater.* **2013**, *25*, 1563 – 1569; d) H. J. Song, D. H. Kim, E. J. Lee, S. W. Heo, J. Y. Lee, D. K. Moon, *Macromolecules* **2012**, *45*, 7815 – 7822; e) I. Osaka, M. Akita, T. Koganezawa, K. Takimiya, *Chem. Mater.* **2012**, *24*, 1235 – 1243; f) Y. Liang, Z. Tao, J. Chen, *Adv. Energy Mater.* **2012**, *2*, 742 – 769; g) T. Zhou, T. Jia, B. Kang, F. Li, M. Fahlman, Y. Wang, *Adv. Energy Mater.* **2011**, *1*, 431 – 439.

[8] a) M. Yao, H. Senoh, T. Sakai, T. Kiyobayashi, *Int. J. Electrochem. Sci.* **2011**, *6*, 2905 – 2911; b) M. Pasquali, G. Pistoia, T. Boschi, P. Tagliatesta, *Solid State Ionics* **1987**, *23*, 261 – 266.

[9] a) H. G. Wang, S. Yuan, D. L. Ma, X. L. Huang, F. L. Meng, X. B. Zhang, *Adv. Energy Mater.* **2014**, *4*, DOI: 10.1002/aenm.201301651; b) Y. Liang, P. Zhang, J. Chen, *Chem. Sci.* **2013**, *4*, 1330 – 1337.

[10] X. Han, C. Chang, L. Yuan, T. Sun, J. Sun, *Adv. Mater.* **2007**, *19*, 1616 – 1621.

[11] C. G. Wang, D. Chen, W. P. Chen, S. Y. Chen, K. Q. Ye, H. Y. Zhang, J. Y. Zhang, Y. Wang, *J. Mater. Chem. C* **2013**, *1*, 5548 – 5556.

[12] E. F. Paulus, F. J. J. Leusen, M. U. Schmidt, *CrystEngComm* **2007**, *9*, 131 – 143.

[13] T. M. Cooper, D. M. Krein, A. R. Burke, D. G. McLean, J. E. Haley, J. Slagle, J. Monahan, A. Fratini, *J. Phys. Chem. A* **2012**, *116*, 139 – 149.

[14] A. Criado, D. Pena, A. Cobas, E. Guitian, *Chem. Eur. J.* **2010**, *16*, 9736 – 9740.

[15] a) W. Ai, Z. Luo, J. Jiang, J. Zhu, Z. Du, Z. Fan, L. Xie, H, Zhang, W. Huang, T. Yu, *Adv. Mater.* **2014**, *26*, 6186 – 6192; b) W. Ai, J. Jiang, J. Zhu, Z. Fan, Y. Wang, H, Zhang, W. Huang, T. Yu, *Adv. Energy Mater.* **2015**, *5*, 1500559.

[16] Z. Song, H. Zhan, Y. Zhou, *Chem. Commun.* **2009**, 448 – 450.

[17] H. Chen, M. Armand, G. Demailly, F. Dolhem, P. Poizot, J.-M. Tarascon, *ChemSusChem* **2008**, *1*, 348 – 355.

[18] C. T. Lee, W. T. Yang, R. G. Parr, *Phys. Rev. B* **1988**, *37*, 785 – 789.

[19] Gaussian 09, Revision A, M. J. Frisch, G. W. Trucks, H. B. Schlegel, G. E. Scuseria, M. A. Robb, J. R. Cheeseman, G. Scalmani, V. Barone, B. Mennucci, G. A. Petersson, H. Nakatsuji, M. Caricato, X. Li, H. P. Hratchian, A. F. Izmaylov, J. Bloino, G. Zheng, J. L. Sonnenberg, M. Hada, M. Ehara, K. Toyota, R. Fukuda, J. Hasegawa, M. Ishida, T. Nakajima, Y. Honda, O. Kitao, H. Nakai, T. Vreven, J. A. Montgomery, Jr., J. E. Peralta, F. Ogliaro, M. Bearpark, J. J. Heyd, E. Brothers, K. N. Kudin, V. N. Staroverov, R. Kobayashi, J. Normand, K. Raghavachari, A. Rendell, J. C. Burant, S. S. Iyengar, J. Tomasi, M. Cossi, N. Rega, J. M. Millam, M. Klene, J. E. Knox, J. B. Cross, V. Bakken, C. Adamo, J. Jaramillo, R. Gomperts, R. E. Stratmann, O. Yazyev, A. J. Austin, R. Cammi, C. Pomelli, J. W. Ochterski, R. L. Martin, K. Morokuma, V. G. Zakrzewski, G. A. Voth, P. Salvador, J. J. Dannenberg, S. Dapprich, A. D. Daniels, Ö. Farkas, J. B. Foresman, J. V. Ortiz, J. Cioslowski, D. J. Fox, Gaussian, Inc., Wallingford CT, **2009**.

[20] J. F. Zhao, J. I. Wong, C. Wang, J. Gao, V. Z. Y. Ng, H. Y. Yang, S. C. J. Loo, Q. Zhang, *Chem. Asian J.* **2013**, *8*, 665 – 669.

Manuscript received: December 9, 2015
Revised: December 28, 2015
Accepted Article published: December 30, 2015
Final Article published: January 21, 2016